Pushbroom imaging spectrometer with high spectroscopic data fidelity: Experimental demonstration

Pantazis Mouroulis and Michael M. McKerns*
Jet Propulsion Laboratory, California Institute of Technology
Pasadena, CA 91109

Abstract

Experimental results are described from a pushbroom imaging spectrometer module demonstrating very low levels of spectral and spatial distortion, at the level of a few percent of a pixel, and similarly small variation in spectral response function with field position. These spectrometer attributes make possible the extraction of accurate spectroscopic information. The spectrometer can achieve high levels of performance despite relaxed tolerances in fabrication and alignment. A quick and effective alignment method is described, that permits the spectrometer to approximate its design performance. The implications of the results on the calibration techniques of pushbroom imaging spectrometers are also discussed.

Subject Terms: imaging spectroscopy, hyperspectral imaging, optical design, distortion, calibration

1. Introduction

Pushbroom imaging spectrometers are a desirable form for Earth observations from space, since they can achieve a higher signal-to-noise ratio than their whiskbroom counterparts. At the same time, they carry the penalty of increased calibration difficulty. While in a whiskbroom spectrometer all pixels have their spectra recorded by the same one linear photodetector array, for a pushbroom spectrometer with 700-1000 spatial pixels there are effectively that many different linear arrays or spectrometers in need of calibration.

The need for accurate calibration of Earth-looking hyperspectral sensors has been recently recognized.[1] Both the peak location of the pixel spectral response function (SRF) and its halfwidth (as well as shape) must be known to within a small fraction of the nominal pixel bandwidth, typically less than a few percent. Translated in pushbroom spectrometer terms, this requirement means that distortion along the spatial direction (called 'smile') as well as the spatial variation of the optical PSF must be kept to a minimum, typically a small fraction of a pixel. Smile is defined here as the deviation from straightness of the monochromatic image of the slit.

Even if errors induced by the above factors could be taken into account during calibration, it would still be best not to have such errors since the computational complexity of data reduction might otherwise increase beyond practical limits. But there is also another practical reason for insisting on relative invariance of the SRF peak location with field, and it has to do with calibration procedure. Measurement of the peak location of the SRF for a pushbroom sensor is complicated because it requires an accurately calibrated monochromator. Such calibration is possible only over a small part of the monochromator slit (essentially a point), because the available monochromators suffer from considerable smile, thus causing an uncertainty in the

*Present address: Department of Physics, University of Alabama,

absolute wavelength. Translation of the monochromator up and down the slit of the test spectrometer is a laborious experimental procedure of doubtful accuracy. Therefore, it is easier to rely on an independent smile measurement from which the SRF peak locations can be inferred. Ideally, such measurement would show lack of smile, hence allowing the same SRF peak location to be used independent of spatial position. Even if the SRF shape is not spatially invariant, its relative shape can be measured with much greater ease than the absolute peak location. Hence simple methods of eliminating as well as measuring smile are of importance.

In addition to the above noted restrictions on the SRF variation, it is also desirable to reduce the distortion along the spectral direction (called 'keystone'). Keystone is caused by the difference in slit magnification with wavelength, but it is measured here as an absolute length value (or fraction of a pixel). This error means that the amount of mixing of the spectra from spatially adjacent pixels will vary with wavelength. This impacts the recovered spectrum of pixels located close to sharp boundaries in the image, or for targets that are less than a few pixels large. The keystone error must be controlled at the level of a small fraction of a pixel, although a more relaxed tolerance of less than about 0.1 pixel can apply here.[2]

This paper contains the description and performance tests of an imaging spectrometer module, which was designed and built in order to verify that small levels of distortion are possible to achieve in practice, and in order to develop the techniques for doing so. It is shown that high levels of performance can be achieved with a simple and compact optical design. The prototype approaches the 2% level in smile and ~7% level in keystone (limited by measurement accuracy). It may be worth repeating that these percentages refer to the pixel size and not to the total field size, as is more common in optical design. To our knowledge, this is the first time that a system is demonstrated to achieve these low levels of error in practice. For example, an evaluation of commercial spectrometers as well as a specially designed unit similar to the one described here revealed smile and keystone errors on the level of one pixel.[3] We are concerned here with a further one-to-two orders of magnitude reduction of these errors.

2. Spectrometer Design

The spectrometer is of the Offner form,[4,5] which has been used previously in space applications.[6] The full potential of the Offner form is now being realized thanks to recent developments in convex grating fabrication by electron-beam (EB) lithography.[7] Alternative Offner spectrometer forms utilizing prisms have been proposed,[8] but a grating-based all-reflective system is simpler and more robust if an efficient and low-scatter convex grating can be had. Several design forms have been described that achieve in theory low levels of distortion.[9] A preliminary report on the spectrometer described here has also appeared.[10] In this paper, we expand the preliminary results of ref. 10 to encompass both smile and keystone, provide full experimental results of the spectrometer performance, and discuss in detail the alignment technique that enables the high level of performance to be easily achieved in practice.

2.1. Specification and prescription data

The basic specifications are given in Table 1. The spectrometer was originally designed as an f/2.8 system with a ~1cm slit (nominal 1024 spatial pixels of 10μm size. A compromise CID array (CIDTEC 3710D) focal plane was used mostly for budgetary reasons.

The design schematic is shown in figure 1a (y-z view) and figure 1b (x-z view). The design prescription is given in Table 2. The slit is displaced by 33.24 mm from the system axis. All mirrors are spherical and with a common axis of symmetry. Primary and tertiary have also been

made concentric, which facilitates alignment. No tilts or decenters are used. All design and evaluation was done using ZEMAX.[11]

Grating characteristics are given in Table 3. The grating is a single blaze design, with the blaze peak at around 575 nm. Detailed efficiency tests were not performed on the grating, but several similar gratings have been made consistently with >87% peak first order relative efficiency.[7] In any case, the efficiency itself is of no importance for this paper. A rather more critical characteristic of the grating is that the blaze angle remains constant across its extent (relative to the local surface normal). This characteristic, enabled by the EB fabrication technique, combines with the small variation of incidence angles that is inherent in the design to produce a grating that has approximately constant diffraction efficiency across its entire aperture. This means that the grating can be modeled in a simple manner, without the need for introducing complicated wavelength-dependent apodization factors.

2.2. Design performance.

Since the design has nearly diffraction-limited performance, we must use diffraction-based metrics. The various performance parameters are summarized in Table 4. The smile is measured as the maximum difference in the x-coordinate of the PSF centroids. Other parameters are self-explanatory.

3. Fabrication and alignment

3.1. Tolerancing and component tests.

Tolerance analysis of the initial design revealed that two of the three mirror curvatures could be fitted to manufacturer's testplates (primary, grating). The curvature of the tertiary and the spacings were then used as variables to reoptimize performance. This resulted in an increase in smile from practically zero to the above quoted 2% of pixel. The tolerance of the tertiary radius was set at 0.1%. Other mirrors were toleranced at two fringes power and 0.5 fringe irregularity. Those tolerances have a negligible effect on performance (change in merit function by a few percent, using the final distance as compensator).

The mirrors and grating substrate were fabricated on fused silica and coated with Al. The primary and tertiary had less than 0.1 wave p-v error over the beam footprint. An interferogram of the grating was very hard to obtain in the zero order because of the miniscule amount of light remaining in that order - the interferometer could not acquire the fringes for automatic analysis. However, sufficient fringe contrast was obtained to ascertain the surface quality visually. Again, the surface irregularity was estimated to be <0.1 wave. An interferogram in the first order was easy to obtain, but it shows considerable off-axis astigmatism as expected. The zero-order (rather than the 1st order) result is representative of what the grating substrate contributes to the overall Offner error, since the astigmatism is at least partly compensated by the rest of the optics.

3.2. Optics alignment.

The following optics alignment method has been developed. The complete method is specific to Offner spectrometers with either a combined primary/tertiary or with separate but concentric primary and tertiary (both spherical). However, some of the steps apply in more general cases as well. It is noted that the Offner design often allows the mirrors to be concentric without any serious penalty and that the use of tilts or decenters in the design is rarely justified. Thus the

designer should strive to achieve concentricity, which will permit easier alignment of the primary and tertiary and may allow them to be easily manufactured as a monolithic block.

First, the primary and tertiary were coarsely positioned. Fine positioning was achieved interferometrically. Using a fast focusing lens at the interferometer, both mirrors are illuminated simultaneously and the zero-fringe position is determined for the portion of the wavefront returned by each mirror. When less than half a fringe is seen on both halves, the mirrors are concentric to that accuracy. This adjustment is done manually and its accuracy is more than adequate.

With the primary and tertiary thus fixed, and with the interferometer focus at their common center of curvature, the entire spectrometer is translated laterally by the amount dictated by the prescription in order to bring the interferometer focus to the middle of the hypothetical slit. At that point, the actual slit may be positioned so as to let the interferometer beam pass without any vignetting. If the slit location is not coincident with the common center of curvature (in terms of its z-coordinate value) then translation along z will also be needed. Generally, the tolerance for slit defocus is good, so the nominal accuracy of a manual micrometer-driven stage suffices for this last adjustment.

The interferometer focus is now at the middle of the slit location. The grating is then coarsely positioned. A return concave mirror is used to test the entire Offner in double pass. First, the grating is clocked (rotated about z) in an approximate way by looking at the image of the diffracted orders and making those nominally horizontal. The correct order is identified for returning with the mirror.

A series of interferograms of the complete system in double pass are then taken while adjusting the grating position and tilt. The aim is to reduce the wavefront error to the minimum possible, depending on individual mirror surface quality. The grating position thus determined is not the final but only an intermediate one. It has been found that the grating tilt/decenter controls the amount of coma, while the z-location controls the astigmatism. Thus the grating alignment is best achieved by first minimizing coma using grating tilt or decenter adjustment only, and then by minimizing astigmatism using the z-translation.

The minimum p-v error that was achieved was 0.24 wave and was consistent with the mirror quality and individual mirror interferograms. The amount of coma and astigmatism was down to about 0.1 wave.

At this point, the optical design software is used in order to simulate the minimum wavefront error configuration for the center of the slit that was determined as above. This is done by merely varying the z-position of the grating through the software. This minimum wavefront location is not the final one because the spectrometer has been optimized for minimum distortion as well as a balanced image quality over all field points. The position of the grating thus determined by the software is then compared with the final design prescription. The grating is finally translated along the z-axis by the difference between the two locations (or better, by observing the amount of astigmatism induced and arriving at the desired value). In the case at hand, the required motion was in the range of 30-40 μm, resulting in an increase in astigmatism to 0.4 wave, which was close to the design value for the f-number used. We note here that it is necessary to arrive at the minimum wavefront error position first because a given amount of astigmatism can be induced by a forward as well as backward movement of the grating, so one does not know which of the two positions is correct unless the above procedure is followed.

The resulting interferogram is shown in figure 2. All wavefront errors in this section refer to a f/no of 3.2 (rather than the minimum design f/no of 2.8), which was determined by the focusing lens used in front of the interferometer. The p-v error is 0.51 wave. The corresponding wavefront generated by ZEMAX for these conditions is shown in Fig. 3, as having an almost purely astigmatic p-v error of 0.5 wave, and can be compared with the wavefront shown in Fig. 3. The middle bump seen in Fig. 3 is due to mirror surface irregularity.

Next, the slit was aligned to vertical. This was accomplished by translating the entire spectrometer vertically and ensuring that the focused spot from the interferometer passed through the slit unvignetted during the entire travel. Two more interferograms were taken at the edges of the slit. The resulting wavefronts differed by ~0.1 wave p-v from the expected values. These two interferograms confirmed that the spectrometer has better image quality (less astigmatism) at the edges of the slit than at the center, as was expected from the design data.

The focal plane is then aligned by observing the image of the slit illuminated with various spectral lamps, as discussed in the smile measurement section below. The optics alignment is then complete except for precise grating rotational alignment (clocking). It is imperative that this adjustment be achieved without disturbing the previous alignment, and the equipment needs to be designed so as to permit that. Otherwise, a movement of the grating necessitates realignment using the interferometer.

This alignment method has been found quick and repeatable. It was possible to realign the entire spectrometer (with the exception of the focal plane) within a few hours, starting from near arbitrary mirror positions. The method allows us to achieve a specified wavefront error rather than a minimum error, and thus determine the minimum distortion position without actually measuring the distortion.

4. Tests

4.1 Dispersion test

The extra spectral pixels of the camera permitted recording of the zero order, which provided a convenient reference point. ZEMAX was used to determine the expected distance between the zero order and various spectral lines. This distance was then converted into pixels, and gave a predicted pixel location for any one wavelength. An unidentified spectral lamp was used to illuminate the slit, to make the test more exciting. The positions of the five spectral lines observed in the range 690-850 nm were compared with the expected positions from a list of five candidate lamps. They were all found to be within a half pixel from their expected location if the unidentified lamp were supposed to be the Argon one.

4.2. Smile measurement

The method for measuring smile is simple. A slit is imaged on the focal plane and illuminated by various spectral lamps at specified wavelengths. The spectral lamp was vertical and a lens was used to image the lamp onto the slit at a nominal 1:1 magnification. With this arrangement, it was found that the measured smile and even line rotation depended on the illumination (e.g. focus, lamp tilt, etc.), implying a less than uniform illumination of the slit, even across its width. A diffuser was then inserted in the middle of the path, near the lens, that is, about equidistant from the slit and the lamp. This was found to eliminate the dependence on the illumination and made the measurement possible. However, the light level was such that only a few strong lines could be recorded.

A high-quality slit is needed. Ours was fabricated by EB lithography. Commercially purchased ruled slits were too irregular or not sufficiently straight. The slit used was two pixels wide. It was also found that only isolated spectral lines could be used reliably. In other words, at least two noise pixels (preferably 3 or 4) are needed before the next spectral line starts.

The monochromatic image of the slit was recorded by the array (along a row). A simple centroiding calculation was then performed along each column, over approximately ten pixels, spanning the image of the line. The resulting centroids (approximately 750, same in number as the spatial pixels of the array) were then plotted with appropriate trendlines. A straight non-horizontal line indicates net rotation. A curved line indicates smile or similar distortion. This method is used also to align the array rotationally with respect to the slit.

Figures 4, 5 show the results achieved for two different spectral lines: the 546.1 Hg line and the 912.3 Ar line. Taking the smile to be the difference between the two interpolated lines (quadratic and linear), we determine a smile of ~2% of pixel, consistent with the design value. But the agreement is not perfect, because according to the design data, the smile is not supposed to turn into a frown at the long wavelength end. Two more lines were recorded, a 435 nm Hg and a 760 nm Kr. Those lines also showed a smile level of less than 2%, but the net slope was not always consistent, varying between +1% and –1%. The measured variation in slope as well as the unexpected change from smile to frown implies that the accuracy of these measurements is of the same order as the measured smile. Of course one may keep in mind that we are attempting to measure extremely small values of smile and rotation (1% of a pixel is 0.13 μm, across a field of 750 pixels or 9 mm).

The results of figures 4 and 5 represent the average of four frames in order to reduce noise. Background frame subtraction was tried but was not found to be useful as it increased the noise. It seemed preferable to shield the stray light sufficiently in a darkened room. Also, pixel sensitivity calibration was not performed. This was not deemed necessary because of the large number of pixels that are involved in the centroiding and the trendline calculation. In any case, the results were found to be independent of the location of the spectral line on the array, and repeated measurements over the same area did not reveal substantial systematic errors.

4.3 Keystone measurement

Keystone is measured by imaging a pinhole that is illuminated by a nominally white source (a tungsten-halogen bulb which was imaged at ~1:1 on the pinhole). This results in a spectrum that forms a line along a column of the focal plane. Centroiding can be performed in a way similar to that described in the previous section, but in the orthogonal direction. Interpolated trend lines can then be compared for tilt or curvature when the pinhole is located at various positions along the slit. The following conditions were needed for a successful measurement.

i. A flattening spectral filter (CVI EQ-2x2) was found useful. This filter is specifically tailored to equalize the combined response of a CCD and a tungsten source. Use of the filter increases the number of usable pixels by effectively increasing the dynamic range of the camera.

ii. The optimum size of the pinhole was found to be at or below the diffraction limit of the system. A small pinhole eliminates any errors caused by the pinhole shape as well as the illumination. The penalty is reduced light level and increased noise, but it is somewhat ameliorated by the fact that no diffuser is needed if the pinhole is so small.

iii. The last few pixels in the blue and IR ends of the spectrum cause unreliable results because of the very low signal level. Only the central 150 pixels out of the 180 total spectral pixels were counted, hence the keystone from one end of the spectrum to the other could be expected to be greater by ~17% of the measured value.

iv. A fourteen-frame average was taken within approximately two seconds. The resulting reduction in scatter was significant.

v. The tilt of the spectrum relative to the array (indicating imperfect clocking of the grating) meant that a large number of noise pixels had to be included on both sides of the line. The centroiding was generally done with more than twenty pixels.

The results are shown in figures 6, 7. Figure 6 shows the spectra obtained for four approximately equispaced pinhole locations spanning the entire slit. The figure shows that the clocking of the grating is not the best possible, since there is an average rotation of 0.10-0.12 pixel from end to end. Two of the four trendlines are practically identical, but the other two show significant difference.

The precision of the grating clocking is limited by the keystone error. Figure 7 shows the net keystone as the maximum difference between any two data sets from Fig. 6. This is net keystone in the sense that if one of the two data sets is perfectly oriented along the array, the other will show the indicated amount of slope. This way of displaying the data removes the effect of the imperfect grating clocking. Fig. 7 shows a net keystone error of just under 7%, which can be extrapolated to ~8.2% in order to include the previously excluded pixels at the ends of the spectrum.

The maximum difference does not occur between the two ends of the slit, but between an intermediate position and one end. This is a possible clue that the measured keystone may represent a limitation in the accuracy of the measurement method. Thus, it is not possible to say with certainty whether the measurement represents a real effect. It is should be appreciated here that when one is trying to measure the lack of an effect, as is the case for both smile and keystone, the accuracy of the experimental apparatus and method will necessarily always be the limiting factor. In any event, these results demonstrate that the spectrometer is free of keystone error at least at the level of 0.1 pixel. We believe that the measurements were ultimately limited by stray light, and that a complete stray light analysis as well as a careful baffle design would be needed in order to improve the accuracy.

5. Estimation of the SRF variation

The SRF of a pixel is normally measured by varying the input wavelength while recording the response of a specific pixel under test.[12] This results in the image of the slit moving along the focal plane from one end of the pixel to the other. The procedure can be described as a convolution of the slit image with the pixel response. The slit image is itself a convolution of the slit (a rect function) with the optical line spread function (LSF). For the convolution to be valid, we need to assume that the LSF is invariant over the limited range of wavelengths that excite any one pixel, a condition that can be thought of as sufficiently satisfied here. Even though the pixel response can be nonuniform,[13] our aim here is not to calibrate the spectrometer as if it were a flight instrument, but merely to show whether there is any variation in SRF caused by the optical design itself. Hence we have chosen to compute the SRF through the above convolution process by taking the pixel response function to be another rect function of equal width to the slit.

From the interferometric data obtained during alignment of the spectrometer, we can determine the actual spectrometer LSF and use that in place of design data. From the three interferometer images that were obtained, we chose the two that give the maximum difference (worst case). The corresponding LSF's are then convolved with the rect functions as above.

Figure 8 compares the SRF computed using the design LSF data with that computed through the measured LSF for the middle of slit (which gives the worst LSF and widest SRF). It can be seen that the difference is very small, and part of it is due to a half-pixel shift that seems to have occurred between the two data sets, something that cannot be easily avoided in the computations. The experimental and design computed SRFs for the edge of the slit are practically identical and hence not shown here.

For the purposes of this paper, we are concerned with the maximum SRF variation with field position, rather than the absolute SRF shape or width. In this sense, both design and experimental data predict a halfwidth variation of the SRF of less than 3% for the 633 nm wavelength and f/3.2 aperture. But the maximum variation occurs at the short wavelength end, where the aberrations are more significant. The close agreement shown in Fig. 8 allows us to use design data in order to calculate this maximum variation. The result is shown in figure 9, for the maximum spectrometer aperture, f/2.8. It can be seen that the two curves are of slightly different shape, and hence their difference is not easily characterized through the change in halfwidth alone. If we take the latter as sufficient description, we may note that it is less than 5%, and thus would provide the approximately the same data accuracy as the smile of 2% [1]. In any case, the difference between the two SRFs is sufficiently small to be detectable only with very accurate calibration techniques.

6. Conclusions

The experimental results have demonstrated a pushbroom sensor with very small amounts of smile (~2% of pixel) and keystone (<10% of pixel), and good SRF uniformity, within a few percent bandwidth variation. The Offner spectrometer can achieve these low levels of smile and keystone with comfortable fabrication tolerances. A quick and reliable alignment method has been developed. A flight instrument with these characteristics would achieve unprecedented spectroscopic data fidelity from a pushbroom sensor.

Techniques for measuring smile and keystone to small fractions of a pixel were demonstrated. We may not state with certainty that the quoted values of smile and keystone represent measurement inaccuracy or real effects. Though it may be possible to develop alternative, more accurate methods for measuring smile and keystone, the methods described here are simple and have the advantage of utilizing the focal plane for which the spectrometer was designed. Therefore, they can also provide the basis for an on-board calibration system that would serve to ensure accurate calibration of a spectrometer throughout the lifetime of a mission. They would also be sufficiently accurate for the planned pushbroom Offner sensors by NASA and other Agencies, insofar as one can ascertain the expected level of performance of such sensors from current design data.

Referring to the calibration problems mentioned in the Introduction, the following spectral calibration steps for a pushbroom spectrometer would seem reasonable based on the current results:

1) Obtain the SRF of a single row of pixels as accurately as possible. This would include knowledge of the absolute location of the peak of the SRF to the specified accuracy.

2) Perform independent smile measurements. Such measurements may be more accurate if an array with smaller pixel size than the flight focal plane array (FPA) can be used, but this is not necessary unless one needs even greater accuracy than demonstrated here.
3) Accept that the knowledge of the SRF peak location will be limited in accuracy by the measured smile, or use the measured smile to predict the peak location of the SRF if the smile measurement accuracy can be relied upon.
4) Calibrate other rows for SRF bandwidth only. This does not require knowledge of absolute wavelength with a high accuracy.

Acknowledgments

This research was performed at the Jet Propulsion Laboratory, California Institute of Technology, under a contract with the National Aeronautics and Space Administration. We thank Paul Maker, Dan Wilson, and Rich Muller of the JPL Microdevices Laboratory for providing us with the grating and the slits used in this prototype. We also thank David Thomas, Rob Green, Tom Chrien, Jeff Simmonds, and Valerie Duval for technical assistance and the many discussions that culminated in the specifications of this prototype. The support of Jeff Simmonds, Barbara Wilson, and Gregg Vane was crucial for the completion of this project.

Table 1

Spectrometer specifications

F/no	2.8
Pixel size (spatial x spectral)	12 x 13.7 μm^2
Spatial pixels	754
Spectral pixels	185 (0.4-1 μm, 480 available)
Slit magnification	-1
Spectral sampling	3.2 nm

Table 2

Prescription Data (distances in mm)

Surface	Type	Radius	Thickness	Glass
OBJ		Infinity	136.0869	
1	Standard	-135.839	-67.22123	Mirror
STO	Diff. Grating	-68.415	61.48648	Mirror
3	Standard	-130.1043	-130.21365	Mirror
IMA		Infinity		

Table 3

Grating characteristics

Order	+1
Pitch	16.2 μm
Clear aperture	25 mm
Sag	1.1 mm

Table 4

Spectrometer Design Performance*

	Strehl	PSF energy in pixel	MTF (tan.)#	MTF (sag.)&	Smile^	Keystone^
400 nm	0.43-0.84	> 94%	0.86-0.93	0.93-0.95	1.8%	1%
1000 nm	0.85-0.90	> 90%	0.83-0.86	0.84-0.85	1.5%	

* The range of values given in some columns indicates worst to best case as a function of field location.

Along the spectral direction, at the Nyquist frequency.

& Along the spatial direction, at the Nyquist frequency.

^ As fraction of pixel size.

References

1. R. O. Green: "Spectral calibration requirement for Earth-looking imaging spectrometers in the solar-reflected spectrum", Appl. Opt. **37**, 683-690 (1998).
2. P. Mouroulis, D. A. Thomas, T. G. Chrien, V. Duval, R. O. Green, J. J. Simmonds, and A. H. Vaughan: "Trade studies in multi/hyperspectral imaging systems: Final Report" NASA Internal Report, available at http://ntpio.nasa.gov/esto.html (1998).
3. J. Fisher, M. Baumback, J. Bowles, J. Grossmann, and J. Antoniades: "Comparison of low-cost hyperspectral sensors", in *Imaging Spectrometry IV*, M. R. Descour and S. S. Shen eds., SPIE Proc. **3438**, 23-30 (1998).
4. A. Offner: "Unit power imaging catoptric anastigmat", U.S. Patent No. 3,748,015 (1973).
5. L. Mertz: "Concentric spectrographs", Appl. Opt. **16**, 3122-3124 (1977).
6. F. Reininger and 46 coauthors: "VIRTIS: visible infrared thermal imaging spectrometer for the Rosetta mission", in *Imaging Spectrometry II*, M. R. Descour and J. M. Mooney eds., Proc. SPIE **2819**, 66-77 (1996).
7. P. Mouroulis, D. W. Wilson, P. D. Maker, and R. E. Muller: "Convex grating types for concentric imaging spectrometers", Appl. Opt. **37**, 7200-7208 (1998).
8. D. R. Lobb: "Imaging spectrometers using concentric optics", in *Imaging Spectrometry III*, Proc. SPIE **3118**, 339-347 (1997).
9. P. Mouroulis: "Low-distortion imaging spectrometer designs utilizing convex gratings", in *International Optical Design Conference 1998*, L. R. Gardner and K. P. Thompson eds., Proc. SPIE **3842**, 594-601 (1998).
10. P. Mouroulis and D. A. Thomas: "Compact, low-distortion imaging spectrometer for remote sensing", in *Imaging Spectrometry IV*, M. R. Descour and S. S. Shen eds., Proc. SPIE **3438**, 31-37 (1998).
11. ZEMAX Optical Design Program, available from Focus Software Inc., Tucson, AZ.

12. T. G. Chrien, R. O. Green, and M. L. Eastwood: "Accuracy of the spectral and radiometric laboratory calibration of the Airborne Visible/Infrared Imaging Spectrometer (AVIRIS)", in *Imaging Spectroscopy of the Terrestrial Environment*, Proc. SPIE **1298**, 37-49 (1990).
13. D. Kavaldjiev and Z. Ninkov: "Subpixel sensitivity map for a charge-coupled device sensor", Opt. Eng. **37**, 948-954 (1998).

Figure Captions

Figure 1a. Schematic of the spectrometer in the y-z plane. The slit is perpendicular to the plane of the paper. The long wavelength end of the spectrum is at the top.

Figure 1b. Schematic of the spectrometer in the x-z plane. The slit and its image are coincident in this projection.

Figure 2. Measured wavefront from the spectrometer at 633 nm and for the center of the slit. The main aberration is astigmatism. The middle bump is due to mirror figure. The p-v error is 0.51 λ.

Figure 3. Predicted wavefront at 633 nm and f/3.2 for the center of the slit, using the design prescription data. The p-v error is 0.5 λ.

Figure 4. Measurement of smile for the 546.1 nm Hg line. The abscissa is the column number, and the ordinate is the location of the centroid for each column, given in fractional pixel units.

Figure 5. Measurement of smile for the 912.3 nm Ar line.

Figure 6. Spectrum orientation for four different locations along the slit. The average overall tilt of the interpolated lines represents imperfect grating clocking (rotational) alignment. The difference between the lines is indicative of keystone.

Figure 7. Net keystone error, obtained as the maximum difference between any two data sets of Fig. 6.

Figure 8. Experimentally derived (squares) and design SRF (triangles) for the center of the slit and 633 nm wavelength. Both curves refer to the test f-number of 3.2.

Figure 9. SRF's for 400 nm and f/2.8 obtained from design data. The outer curve is the SRF for the middle of the field (worst LSF), and the inner curve is for the field location that gives the best LSF (approximately 85% of full field). The difference between these two curves represents the maximum SRF variation with field expected from the spectrometer.

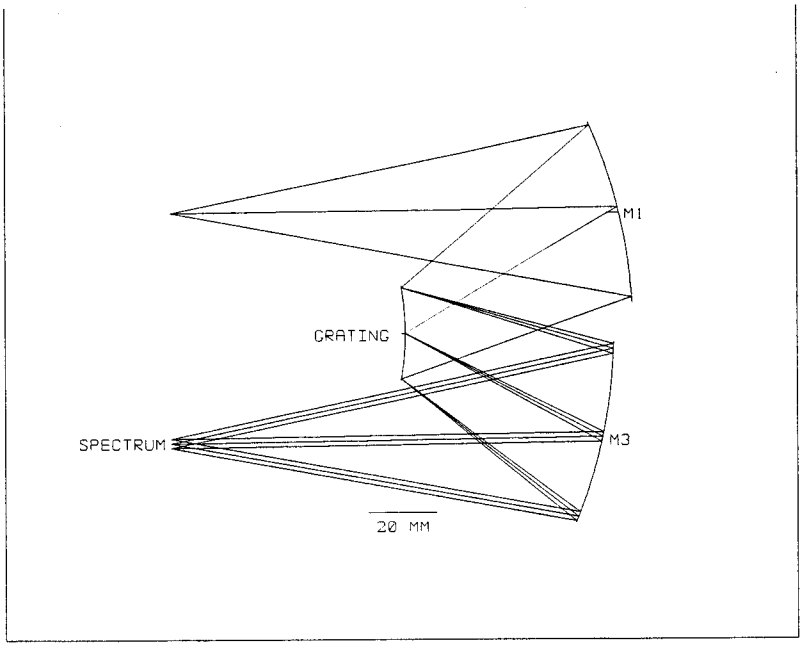

Figure 1 (a)

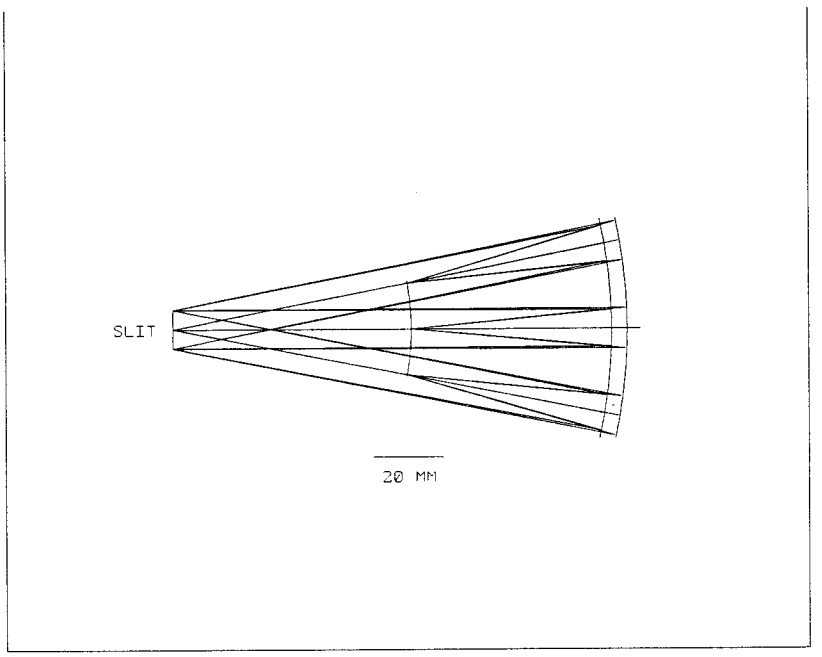

Figure 1 (b)

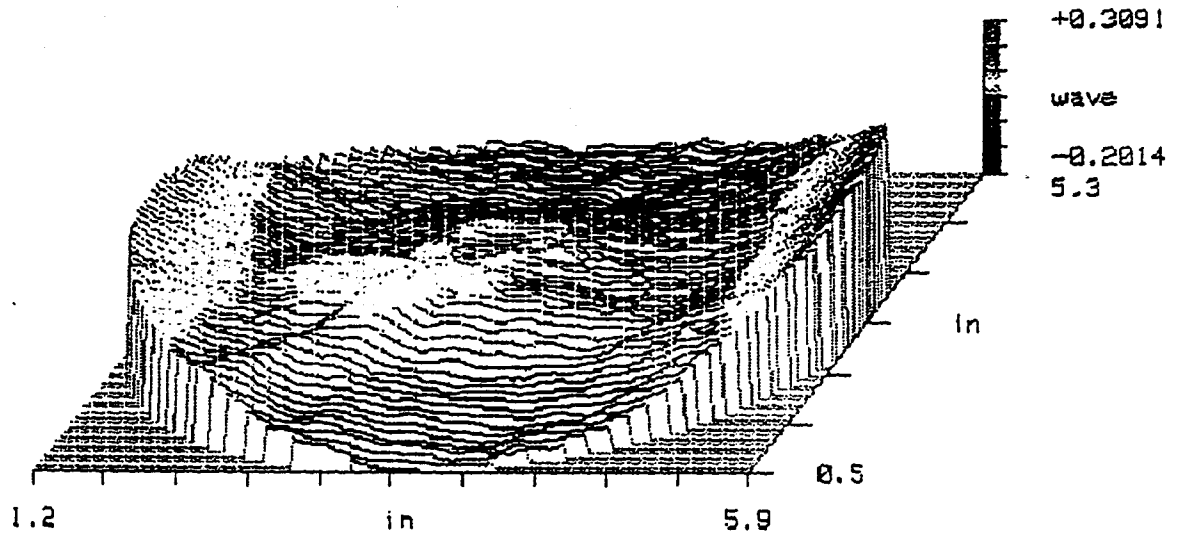

FIGURE 2

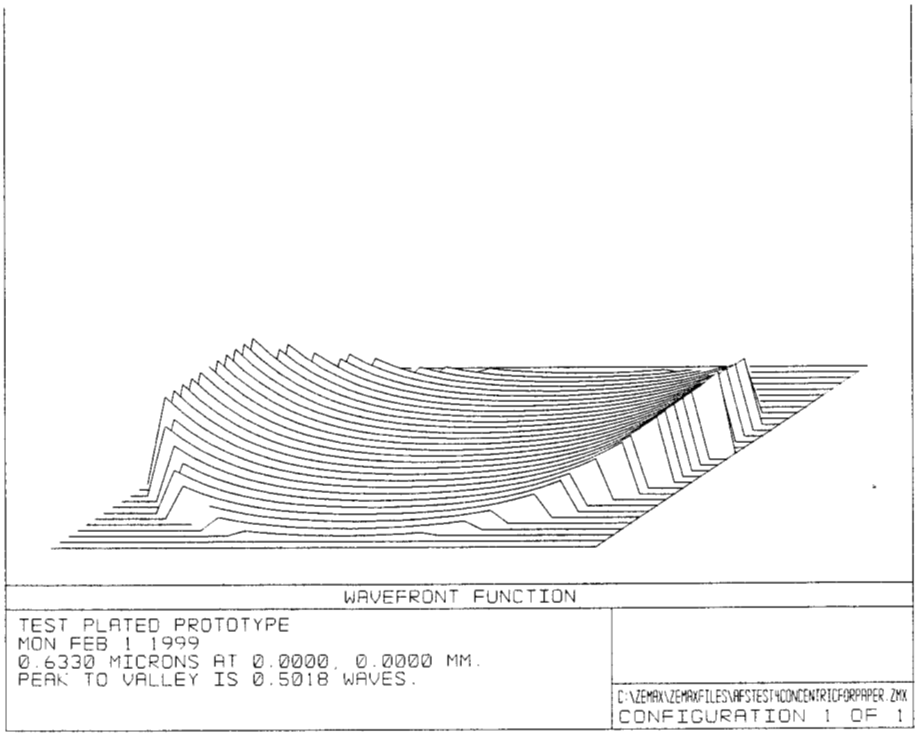
WAVEFRONT FUNCTION
TEST PLATED PROTOTYPE
MON FEB 1 1999
0.6330 MICRONS AT 0.0000, 0.0000 MM.
PEAK TO VALLEY IS 0.5018 WAVES.
C:\ZEMAX\ZEMAXFILES\AFSTEST4CONCENTRICFORPAPER.ZMX
CONFIGURATION 1 OF 1

Figure 3

FIGURE 4

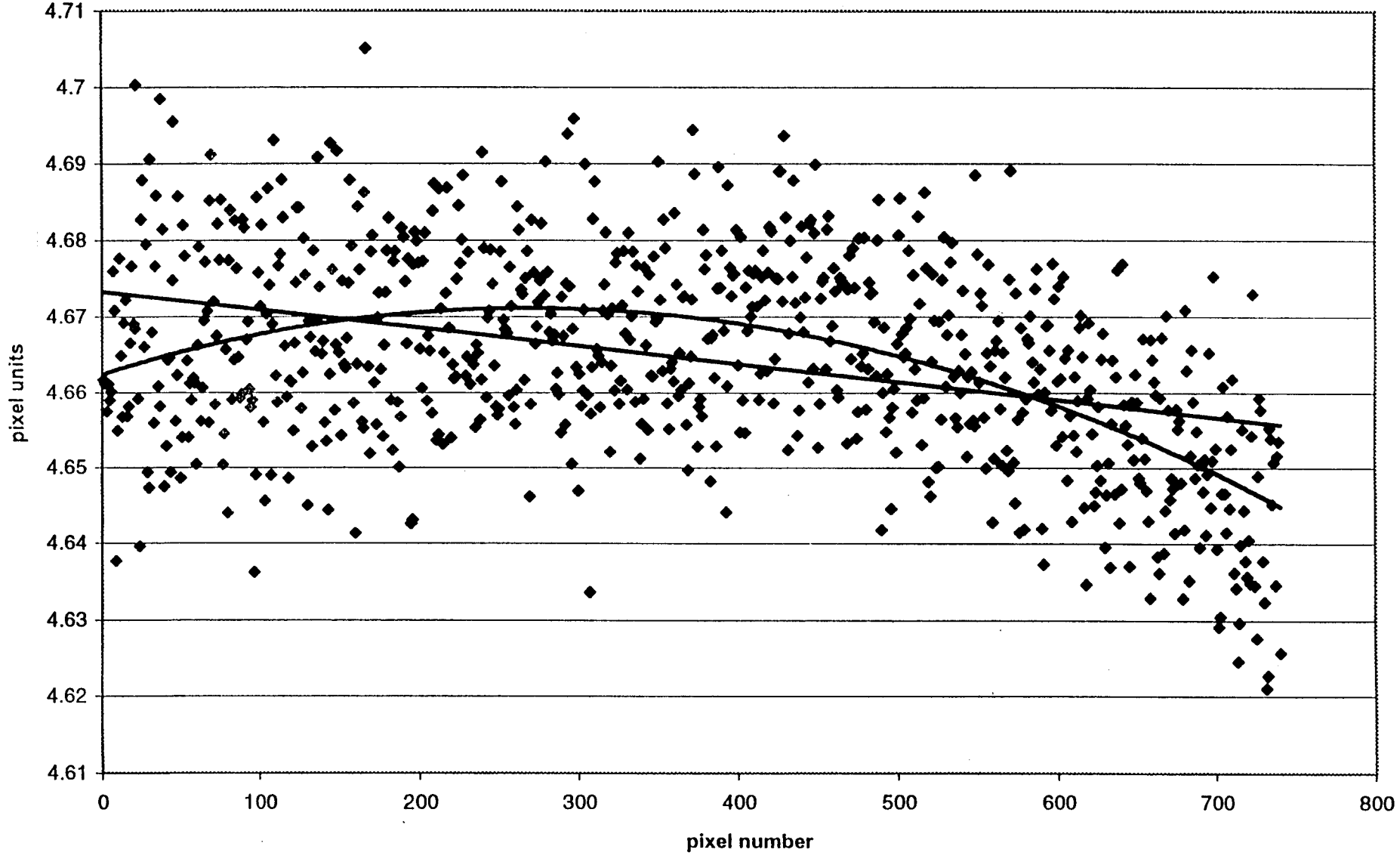
4.71
4.7
4.69
4.68
4.67
4.66
4.65
4.64
4.63
4.62
4.61
pixel units
0
100
200
300
400
500
600
700
800
pixel number

FIGURE 5

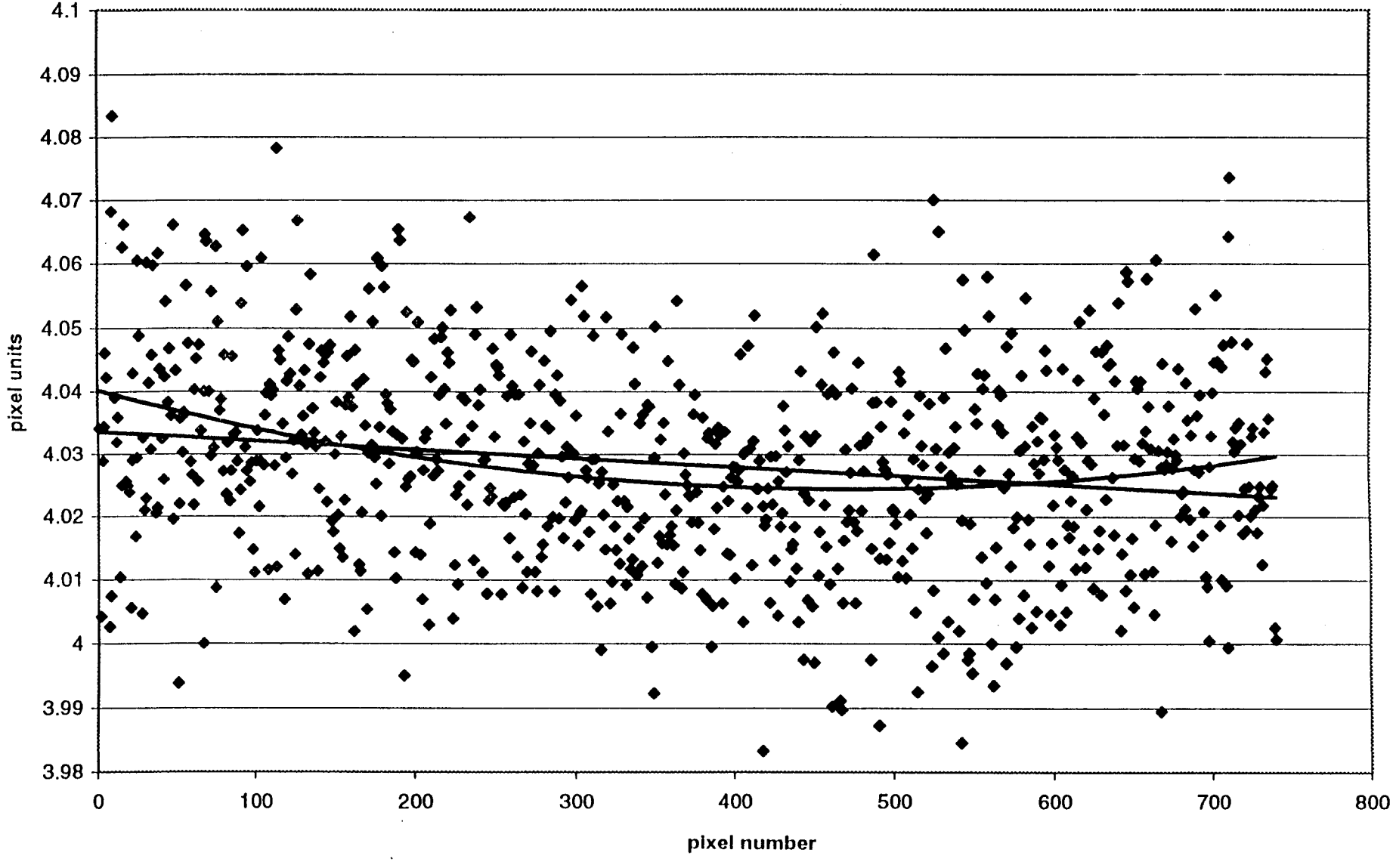
4.1
4.09
4.08
4.07
4.06
4.05
4.04
4.03
4.02
4.01
4
3.99
3.98
pixel units
0
100
200
300
400
500
600
700
800
pixel number

FIGURE 6

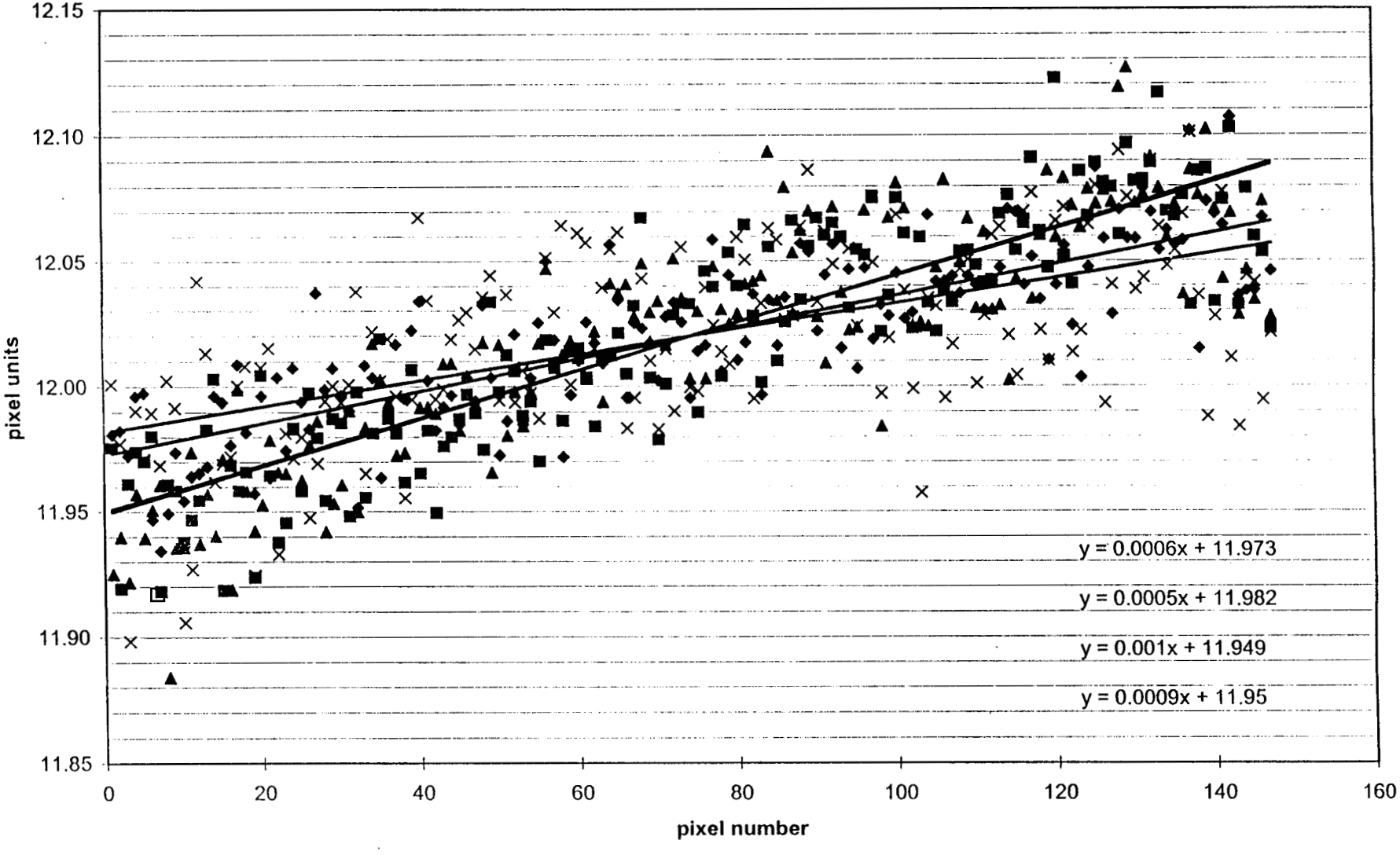
12.15
12.10
12.05
12.00
11.95
11.90
11.85
pixel units
0
20
40
60
80
100
120
140
160
pixel number
y = 0.0006x + 11.973
y = 0.0005x + 11.982
y = 0.001x + 11.949
y = 0.0009x + 11.95

FIGURE 7

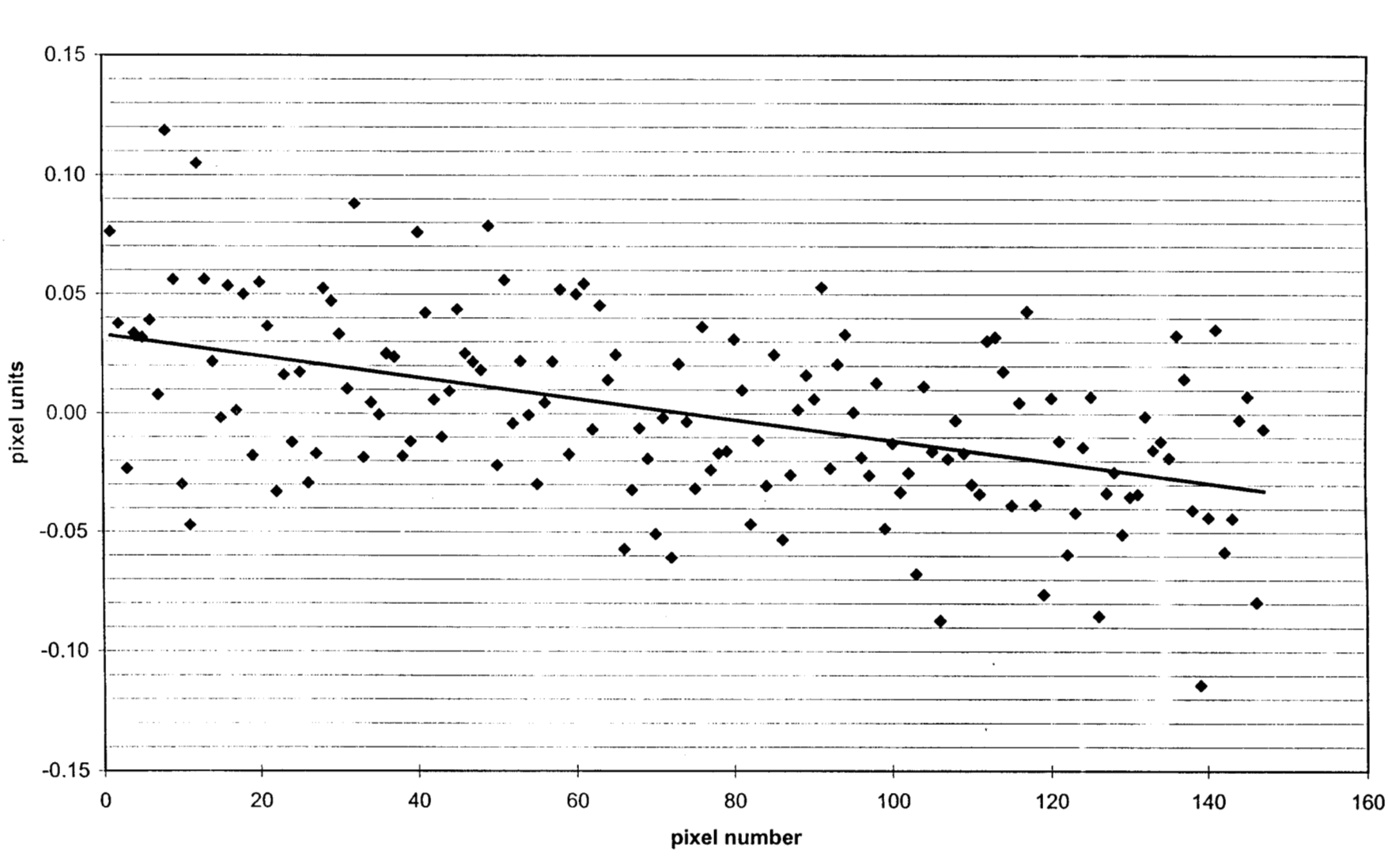
Net keystone
0.15
0.10
0.05
0.00
-0.05
-0.10
-0.15
pixel units
0
20
40
60
80
100
120
140
160
pixel number

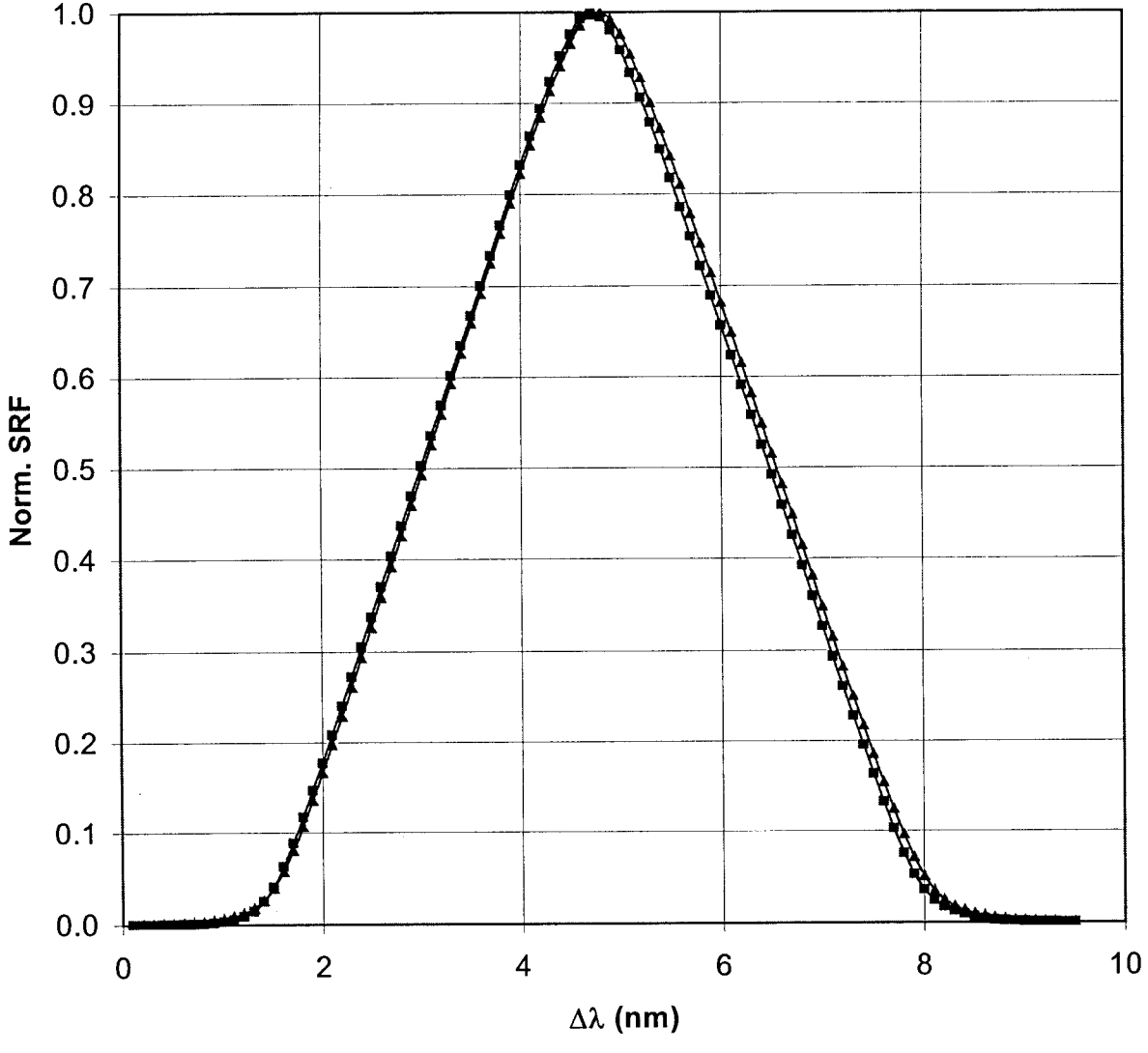

FIGURE 8

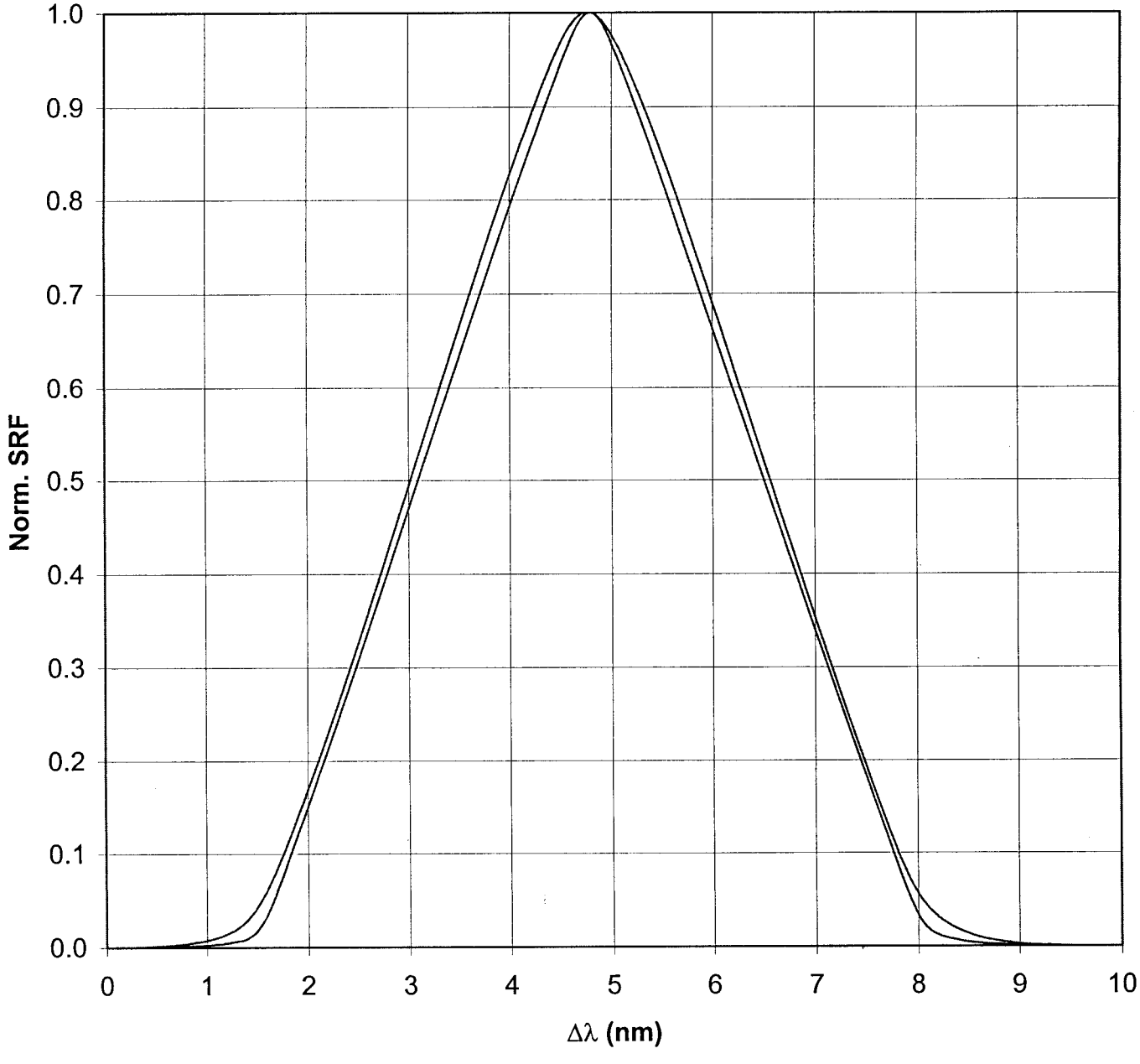

FIGURE 9

PROCEEDINGS OF SPIE REPRINT

SPIE—The International Society for Optical Engineering

Reprinted from

Imaging Spectrometry IV

20–21 July 1998
San Diego, California

Volume 3438

Compact, low-distortion imaging spectrometer for remote sensing

Pantazis Mouroulis* and David A. Thomas*

Jet Propulsion Laboratory
California Institute of Technology
4800 Oak Grove Drive, Pasadena, CA 91109

ABSTRACT

We describe a pushbroom imaging spectrometer having a number of attractive features for remote sensing applications, including compact and simple form, good image quality, high efficiency, and very low levels of distortion. These properties are made possible by the unique characteristics of convex gratings manufactured by electron-beam lithography. A laboratory prototype has been built and is under evaluation. It has an f-number of 2.8, covers a spectral band from 400 to 1000 nm with 3 nm spectral resolution and has 750 spatial elements across the entrance slit. Experimental results are shown that demonstrate very low distortion, on the level of 2% of a pixel.

Keywords: imaging spectrometry, hyperspectral imaging, optical design, distortion, calibration

1. INTRODUCTION

Pushbroom imaging spectrometers are a desirable form for Earth observations from space, since they can achieve a higher signal-to-noise (s/n) ratio than their whiskbroom counterparts. At the same time, they carry the penalty of increased calibration difficulty. While in a whiskbroom spectrometer all pixels have their spectra recorded by the same one linear photodetector array, for a pushbroom spectrometer with 700-1000 spatial pixels there are effectively that many different linear arrays or spectrometers in need of calibration.

It has been recently recognized that the required calibration accuracy must be very high. The spectral response function (SRF) of a pixel must be known accurately. The desired uncertainty in the location of the peak of this function is on the order of 1% (e.g. 0.1 nm in 10 nm pixel bandwidth) in order to produce data that are free of significant spectral calibration errors. A similar tight tolerance applies to the variation of the halfwidth of the SRF.[1]

Translation of these tight calibration requirements to a pushbroom imaging spectrometer leads to a very difficult calibration task if there is any substantial variation of the SRF along the spatial direction. It is thus desirable to reduce such variation to very small levels. There are two consequences for the optical design: 1) the distortion must be controlled to a small fraction of a pixel, and 2) the point spread function (PSF) variation across the field must be small.

We distinguish two errors associated with distortion along the spatial and spectral directions. The first one is that the monochromatic slit image may be curved rather than straight. This is referred to as 'smile', and it is the error associated with the location of the peak of the SRF. The second error, called 'keystone', refers to the fact that the spectrum of any one point on the slit must be parallel to the spectrum of another point. This error does not enter directly into the spectral calibration of a pixel, but it causes mixing of the spectra from adjacent pixels. Though some level of this mixing is unavoidable, the presence of keystone means that the level of mixing varies with spatial location, thus complicating the extraction of information for any one pixel.

* Email: pantazis.mouroulis@jpl.nasa.gov, david.a.thomas@jpl.nasa.gov

In this paper we are concerned primarily with demonstrating low levels of smile and the associated reduction in spectral calibration error. The current state of the art in pushbroom imaging spectrometers has reduced the above distortion errors down to approximately the quarter pixel level (25%), with some (as yet untested) designs claiming levels of about 10% in theory. In this paper, we demonstrate a laboratory prototype which approaches the 2% level, and has the potential for even further reduction. To our knowledge, this is the first time that a system is demonstrated to achieve these low levels of error.

2. THE OFFNER SPECTROMETER

The above requirements can be satisfied using what has come to be known as the Offner spectrometer form.[2,3] This relies on the Offner unity magnification reflective relay, which comprises two spherical concentric reflectors (concave and convex) with the convex one having half the radius of the concave. The following are the advantages of the Offner spectrometer form with a convex grating as dispersive element.

- It can operate at relatively low f-number (greater than about f/2).
- It accepts a long slit while maintaining a highly compact form. Several useful designs have been produced in which the maximum spectrometer dimension is only four to five times the slit length. Since the design is scalable, an absolute slit length specification is not particularly meaningful. However, designs with 25-27mm slit length have been produced, which make use of the maximum possible dimension in IR detector arrays.
- It offers the potential for very small distortion in both spectral and spatial directions if appropriately optimized.
- It has only three (two) optical surfaces (excluding fold mirrors not fundamental to the design form).
- It typically utilizes only spherical and centered surfaces. This feature, in addition to ease of fabrication, provides the best possible chance of approximating the theoretical performance in practice.

Several compact Offner spectrometer designs have been produced spanning the ultraviolet to thermal IR spectral range, while presenting minimum smile and keystone errors, of approximately 1%. These designs are described in ref. 4.

Spectrometer forms based on the Offner relay have been proposed using curved prisms as the dispersing elements.[5] However, the addition of three curved prisms is a considerable complication. A grating-based design is simpler, provided the gratings can be of sufficient quality and of high enough efficiency. These requirements can be satisfied using gratings made by electron-beam lithography.

3. E-BEAM GRATING CHARACTERISTICS

The properties of convex gratings manufactured by E-beam lithography have been detailed elsewhere.[6] We give here a summary of the relevant characteristics.

The grating relief pattern is formed on a thin (~2 μm) layer of PMMA which is spun-coated onto the curved substrate. A reflective Al layer (30 – 50 nm thick) is evaporated on top. Adhesion, thermal cycling, vibration, and outgassing tests have been successfully performed as part of flight qualification.

These gratings can achieve the maximum possible efficiency under any desired spectral response specification. This is because the E-beam technique affords the flexibility of either varying the blaze angle or of keeping it constant across the extent of the grating. Typically, a blazed grating has the highest possible peak efficiency, but may not be adequate at short or at long wavelengths, depending on the width of the desired band. By varying the blaze angle, a broader band can be covered at the expense of peak efficiency. Since the E-beam technique generates the blaze angle of each groove independently by varying the exposure, it is possible to tailor the blaze angle variation to achieve a desired grating spectral response. In addition, coherence can be maintained from one groove to the next or from one panel to the next, unlike ruled gratings which normally show random or uncontrolled phase shifts between panels or areas with

different blaze angles. A relative peak efficiency of around 88% in the first order has been consistently achieved for a single-blaze grating or grating panel. In addition to maximizing efficiency, the E-beam technique affords flexibility in constructing aberration-correcting gratings, or gratings with profiles that differ from the blazed sawtooth type for the purpose of obtaining a specified response.

E-beam gratings have been compared with holographic and ruled gratings of the same specifications, and have outperformed these other types not only in terms of diffraction efficiency, but also wavefront quality and scatter. Further, in terms of achieving the design values of smile and keystone, there are two critical characteristics of these gratings, which cannot be achieved through ruling techniques. These are 1) that the phase shift between panels or different blaze areas is controllable, and 2) that the blaze areas (if more than one) can be made concentric, which minimizes the impact of intensity apodization on the location of the centroid of the PSF and hence on distortion.

4. DESCRIPTION OF THE PROTOTYPE SPECTROMETER

The present device has the following characteristics: spectral range 400-1000nm with nominal 3 nm resolution per pixel (188 spectral pixels), f/2.8, and 750 spatial pixels. Though the optical design can support a greater number of spatial pixels, the limit is provided in this case by the photodetector array (CIDTEC 3710D). This is a nominal 754x484 CID array, with 12x13.7 μm pixels. Thus the maximum recorded slit length is 9 mm. The 400-1000 nm spectrum is recorded over only ~188 out of the 484 spectral pixels, but the extended image can be used to record also the 0^{th} order, thus providing an easy means of wavelength calibration. The array has a fill factor of about 85%, the inactive area being occupied by a ~2 μm Al strip running down the length of a column (along the long direction).

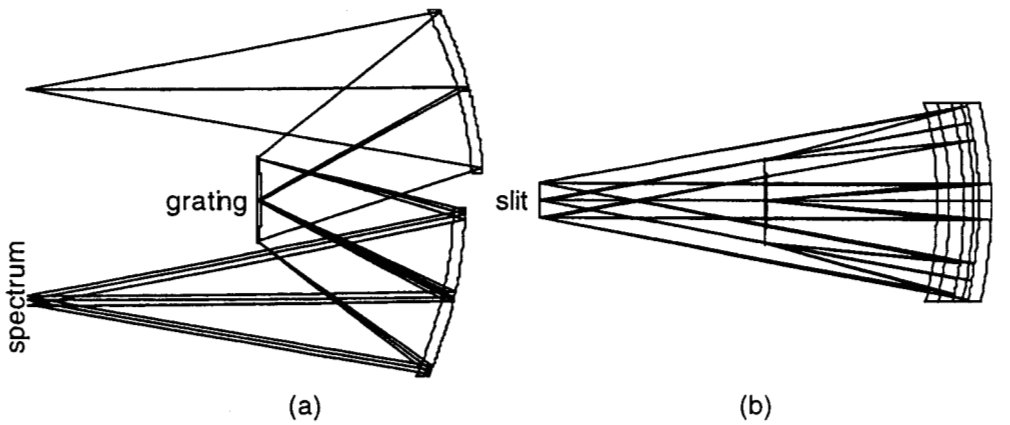

Figure 1. Prototype spectrometer schematic. The scale is approximately 0.5.

The optical design schematic is shown in figure 1. Though it might have been possible to design an even more compact form, the purpose of this prototype was to show that very low smile and keystone values can be achieved in practice, and to develop the necessary alignment and measurement techniques. Tolerance analysis revealed that two of the three curvatures could be fitted to manufacturer's testplates. The curvature of the tertiary, together with the spacings were then used as variables to re-optimize performance. The result of this process was an increase in the design values of smile from practically zero to about 2%, and of keystone to about 1.2%. Both these values were considered within tolerance for this demonstration. The tolerance on the tertiary radius of curvature was set at 0.1%. Other mirrors were toleranced at two fringes power and 0.5 fringe irregularity.

The design has essentially diffraction-limited performance at the long wavelength end (Strehl ratio >0.83), while the ensquared energy within a pixel is about 92%. At the short wavelength end, where the diffraction spread is small, the ensquared energy is even higher, more than 96%, even though the image quality is somewhat degraded. The worst-case point spread function (PSF) is shown in figure 2. This is obtained at 400 nm and at the middle of the slit. It can be seen from figure 2 that the optical PSF is essentially fully contained in the pixel.

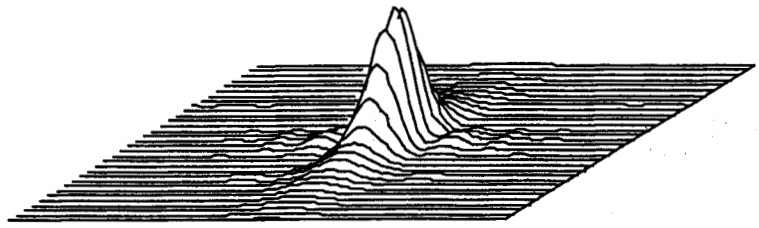

Figure 2. Worst-case PSF for the prototype spectrometer design. The size of the rectangle is approximately one pixel (13 μm). The Strehl ratio for this PSF is ~ 0.42.

Finally, another way to appreciate the image quality is through the system MTF, shown in figure 3. Again, the worst-case MTF only is shown, and it can be seen that the residual aberration has a rather small effect.

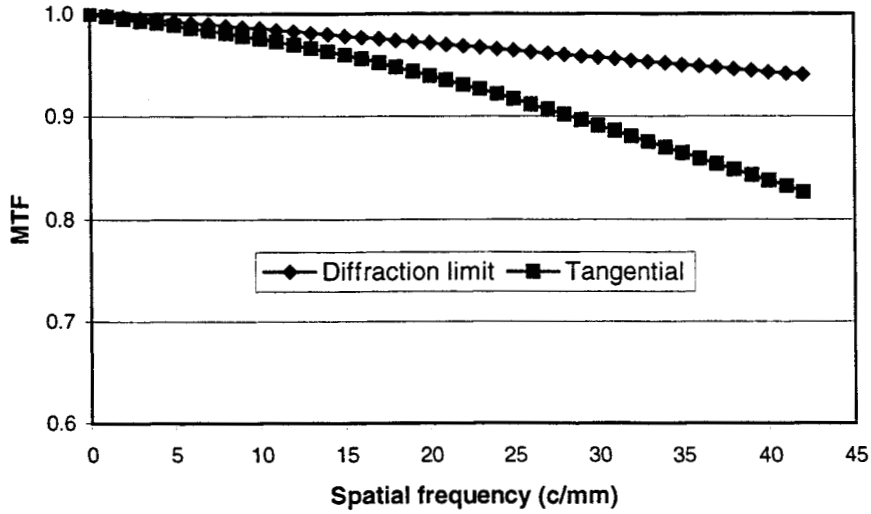

Figure 3. Worst-case design MTF for the prototype spectrometer. The maximum frequency shown corresponds to the Nyquist limit as determined by the detector pixel size.

The grating used for this spectrometer operated in the first order and did not have any partitions (panels), which gives optimum wavefront quality. The blaze angle remained constant relative to the local surface normal, thus providing true blazed grating behavior despite the substrate curvature. Further details of the performance of E-beam gratings are given in ref. 6.

5. ALIGNMENT

The spectrometer was assembled using standard optical laboratory mounts. The mirrors and grating were placed on x-y-z stages. In addition, the grating could be rotated on a goniometric stage in order to orient the grooves along the vertical direction with sufficient accuracy. The camera was placed on a mount with three degrees of freedom in translation as well as rotation.

The first task was to align the primary and tertiary to their common center of curvature. This was done by using an interferometer that illuminated both mirrors, and manually approaching the zero fringe condition for both mirrors simultaneously. This is a simple adjustment, typically accomplished in tens of minutes. The spectrometer was then translated laterally so that the focus of the interferometer beam was placed at the center of the slit location. With the primary and tertiary thus fixed, the grating was then put in place by obtaining several interferograms of the complete spectrometer in double pass. It was found possible to approximate the theoretical performance within two to three hours of adjustment. The optical design software (ZEMAX) generated interferograms that showed 0.8 λ p-v of astigmatism for a point object at the center of the slit and 632.8 nm wavelength. The actual value measured after adjustment was ~0.8 λ p-v of total wavefront error, with the following Seidel terms: 0.5 λ of astigmatism, 0.3 λ of spherical and 0.2 λ of coma. The residual spherical and coma terms are probably a result of mirror surface quality. The fact that the amount of astigmatism is less than the design value implies that the spectrometer was not aligned at exactly the design condition, which, in any case would have been hard to achieve interferometrically. This alignment method accuracy was thought of as sufficient for a start. The optical design model confirmed that the level of smile was not affected by such a small residual misalignment.

6. RESULTS

The smile was measured by using a 28 μm wide slit at the input, illuminated by various spectral lamps. The slit was made through lithographic techniques for maximum accuracy and edge quality. The wavelengths tested were 435 nm (Hg), 546 nm (Hg), 760 nm (Kr), and 912 nm (Ar). Figure 4 shows a representative result obtained for the 546.1 nm Hg line. The figure shows two interpolated curves, linear and quadratic. The linear one represents residual misalignment between the camera and the slit, which can be seen to be at the 2% pixel level. The difference between the two interpolated curves represents the smile inherent in the sensor. It can be seen that this difference is again ~2% of a pixel. Similar results were obtained with the other spectral lines. The 546 nm line gave the highest smile value.

In a real sensor, it would be desirable to minimize not only the smile but also the rotation of the focal plane shown in figure 4. This adjustment would require a more precise rotation stage than the one used for this preliminary experiment.

The simple centroiding calculation used to produce figure 4 assumes that the pixel response (or sensitivity) is uniform at the subpixel level. This is an assumption in need of closer examination, if one is to measure very low values of smile reliably. The detailed mapping of the pixel sensitivity[7] is a laborious process that was not undertaken here, but may be necessary if one seeks the ultimate accuracy and repeatability from these measurements.

The data of figure 4 represent an average of four frames. A larger number of frames tends to reduce the scatter but does not lead to a different shape of the interpolated lines. The errors associated with the measurement are more critically due to the influence of the slit illumination (which must be uniform) and the number of pixels that are averaged on either side of the spectral line. This number may be limited in practice by the presence of adjacent spectral lines. The influence of these factors leads us to estimate the accuracy of the current measurement technique to be similar to the level of smile demonstrated by the sensor.

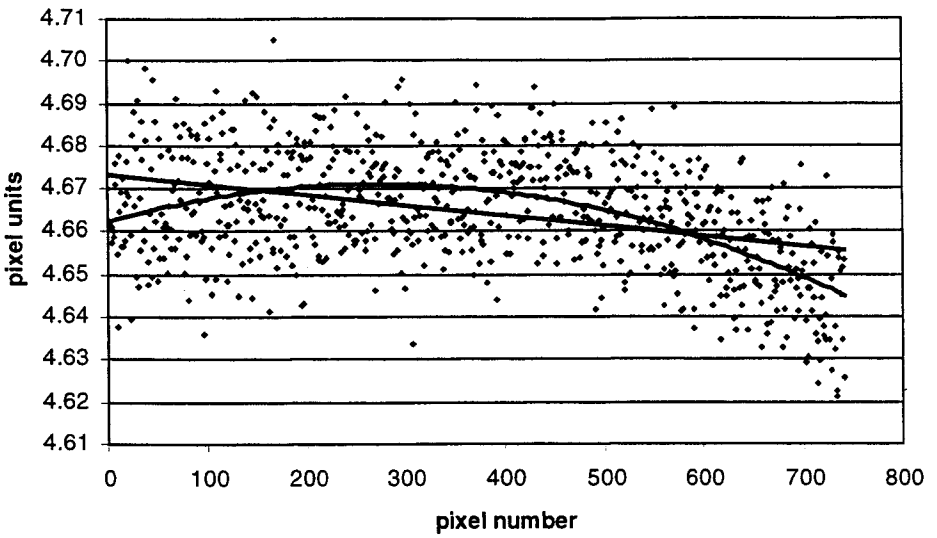

Figure 4. Image of the Hg 546.1 spectral line as obtained with the prototype spectrometer. Each point represents the centroid of approximately ten pixels along a column of the array. The horizontal axis gives the column (pixel) number.

In addition to low smile, the SRF halfwidth variation must remain small. At the time of writing no careful measurements of the SRF variation had been performed. However it is possible to obtain a general idea of what to expect from this spectrometer by using a simple theoretical simulation that simplifies the sub-pixel sensitivity response to a rect function, and also by using the computed diffraction PSF. The maximum SRF variation occurs at the shortest wavelength, where the image quality varies the most. This is shown in figure 5. This variation is quite small because the main lobe of the PSF is still considerably smaller than the pixel for any field location. Thus, although this spectrometer was not specifically optimized to show minimum SRF variation, it should still perform very well in that area. We may note however, that this is in a sense only half a spectrometer in terms of typical spectral coverage for Earth observations. The addition of another module to cover the band 1000-2500 nm would change this design by necessitating a longer slit, since this small pixel size cannot be maintained at longer wavelengths. The achievement of the same performance over the broader spectral band will then pose additional problems, especially if a very compact size is desired. However, the requirement for a longer slit is somewhat balanced by the larger pixel size which permits a greater PSF variation, as well as larger absolute values of smile and keystone. The spectrometer form presented here, with the possible incorporation of an aberration-balancing phase function at the grating, should still be capable of providing excellent performance.

7. CONCLUSIONS AND OUTLOOK

This work has demonstrated a compact pushbroom imaging spectrometer module that can achieve very low values of smile in practice. The importance of low smile is that it reduces considerably the calibration difficulty of a pushbroom imaging spectrometer, because it implies that the center wavelength of the pixel SRF does not have to be measured except for one or two complete columns. The prototype design also exhibits very small SRF bandwidth variation across the field.

Work on this prototype spectrometer has only just begun. Future improvements in data gathering involve automatic averaging of a large number of frames, including frames that are shifted by a few microns at a time relative to each other. This is expected to improve the accuracy and repeatability of the measurements

to the point where a 1% smile should be detectable reliably. The SRF variation must also be measured and compared with the design values. Finally, the level of keystone error must be ascertained, which is expected to be a more complicated measurement than that of smile.

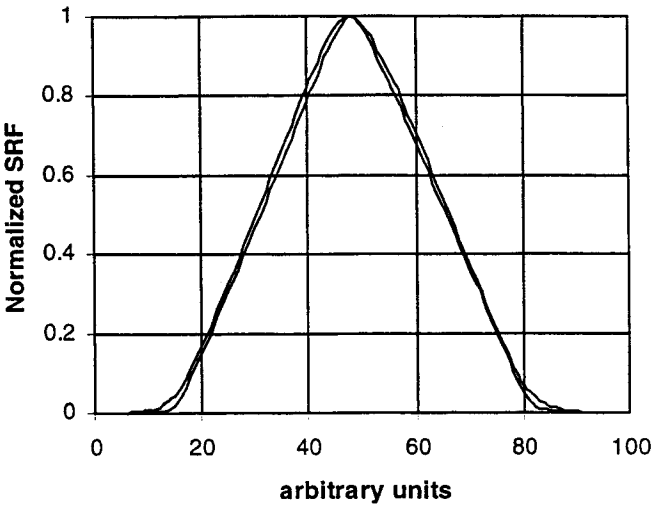

Figure 5. Maximum predicted SRF variation for the prototype spectrometer. The wider curve is the SRF arising from the PSF shown in figure 2. The narrower curve is the SRF from the corresponding best PSF (for a different field position) for the 400 nm wavelength.

8. ACKNOWLEDGMENTS

This research was performed at the Jet Propulsion Laboratory, California Institute of Technology, under a contract with the National Aeronautics and Space Administration. We thank Paul Maker, Dan Wilson, and Rich Muller of the JPL Microdevices Laboratory for providing us with the grating used in this prototype, and Mike McKerns (U. of Alabama, Birmingham) for technical assistance. We also wish to thank Jeff Simmonds, Barbara Wilson and Gregg Vane for their support of this project.

9. REFERENCES

1. R. O. Green, "Spectral calibration requirement for Earth-looking imaging spectrometers in the solar-reflected spectrum", Appl. Opt. **37**, 683-690 (1998).
2. A. Offner: "Unit power imaging catoptric anastigmat", U.S. Patent No. 3,748,015 (1973)
3. L. Mertz: "Concentric spectrographs", Appl. Opt. **16**, 3122-3124 (1977).
4. P. Mouroulis: "Low-distortion imaging spectrometer designs utilizing convex gratings", 1998 International Optical Design Conference (to appear as SPIE vol. 3482).
5. D. R. Lobb: "Imaging spectrometers using concentric optics" in *Imaging Spectrometry III*, Proc. SPIE **3118**, 339-347 (1997).
6. P. Mouroulis, D. W. Wilson, P. D. Maker, and R. E. Muller: "New convex grating types for concentric imaging spectrometers", Applied Optics (in press).
7. D. Kavaldjiev and Z. Ninkov: "Subpixel sensitivity map for a charge-coupled device sensor", Opt. Eng. **37**, 948-954 (1998).